Publication Year	2008
Acceptance in OA	2023-01-26T12:10:18Z
Title	Optical Surface Brightness Fluctuations of Shell Galaxies toward 100 Mpc
Authors	Biscardi, I., RAIMONDO, Gabriella, CANTIELLO, Michele, BROCATO, Enzo
Publisher's version (DOI)	10.1086/587126
Handle	http://hdl.handle.net/20.500.12386/33077
Journal	THE ASTROPHYSICAL JOURNAL
Volume	678

The Astrophysical Journal, 678:168–178, 2008 May 1
© 2008. The American Astronomical Society. All rights reserved. Printed in U.S.A.

OPTICAL SURFACE BRIGHTNESS FLUCTUATIONS OF SHELL GALAXIES TOWARD 100 Mpc

I. Biscardi,[1,2] G. Raimondo,[1] M. Cantiello,[1,3] and E. Brocato[1]

Received 2007 August 7; accepted 2008 February 5

ABSTRACT

We measure F814W surface brightness fluctuations (SBFs) for a sample of distant shell galaxies with radial velocities ranging from 4000 to 8000 km s^{-1}. The distance at galaxies is then evaluated by using the SBF method. For this purpose, theoretical SBF magnitudes for the *HST* ACS filters are computed for single-burst stellar populations covering a wide range of ages ($t = 1.5$–14 Gyr) and metallicities ($Z = 0.008$–0.04). Using these stellar population models, we provide the first $\bar{M}_{\rm F814W}$ versus $({\rm F475W} - {\rm F814W})_0$ calibration and we extend the previous M_I versus $(B-I)_0$ color relation to colors $(B-I)_0 \leq 2.0$ mag. Coupling our SBF measurements with the theoretical calibration we derive distances with a statistical uncertainty of $\sim$8%, and systematic error of $\sim$6%. The procedure developed to analyze data ensures that the indetermination due to possible unmasked residual shells is well below $\sim$12%. The results suggest that *optical* SBFs can be measured at $d \geq 100$ Mpc with *HST* ACS imaging. SBF-based distances coupled with recession velocities corrected for peculiar motion, allow us obtain $H_0 = 76 \pm 6$ (statistical) ± 5 (systematic) km s^{-1} Mpc^{-1}.

Subject headings: galaxies: distances and redshifts — galaxies: elliptical and lenticular, cD — galaxies: photometry

1. INTRODUCTION

The surface brightness fluctuation (SBF) method is a powerful technique to derive distance to galaxies when individual stars cannot be resolved. The method was first introduced by Tonry & Schneider (1988) and is based on a simple concept: the Poissonian distribution of unresolved stars in a galaxy produces brightness fluctuations between pixels of the galaxy image. The resulting pixel-to-pixel variance of the fluctuation is inversely proportional to the square of the distance, and therefore can be used as distance indicator. Although limited by pixel resolution and high S/N ratio, the SBF method showed the capability of spanning an interval of distances extremely wide, ranging from Local Group objects (Ajhar et al. 1994; Raimondo et al. 2005; Rekola et al. 2005) up to galaxies at 100 Mpc (Thomsen et al. 1997; Jensen et al. 2001).

Ideally, SBF measurements can be derived for almost any morphological type of galaxy, provided that the region analyzed has a nearly regular/smooth luminosity profile. Indeed, the presence of morphological irregularities represents a constrain to reliable measurements of SBF, for example, if dusty regions are present, the application of SBF technique requires an accurate masking of dust.

As recognized by Tonry et al. (1990), the properties of the stellar populations in the galaxy cannot be neglected in calibrating the absolute SBF magnitude. This is usually overcome by providing a relation between the SBF magnitude and a galaxy color. Once such a calibration is available, the SBF method can be adopted to infer the distance of elliptical, lenticular, and spiral galaxies with prominent bulge (e.g., Tonry et al. 2001; Mieske et al. 2006; Mei et al. 2007). Moreover, the SBF technique has been successfully applied to low surface brightness dwarf ellipticals (Jerjen et al. 1998, 2000a, 2000b; Rekola et al. 2005), and Galactic or Magellanic Clouds stellar clusters (Ajhar et al. 1994; González et al. 2004; Raimondo et al. 2005).

An interesting case is represented by shell elliptical galaxies, a small number of which are included in the sample observed by Tonry et al. (2001). Shell structures are generally faint and sharp stellar features, and they are considered a robust indicator of past merging or interaction events (Malin & Carter 1983; Wilkinson et al. 2000). The stellar population in the shell depends on the galaxy with which the merger has taken place and on the time spent since the shell structure has formed (Pence 1986; Wilkinson et al. 2000). Many authors have found shells redder or bluer than the underlying galaxy (Forbes et al. 1995; Turnbull et al. 1999; Sikkema et al. 2007).

It is reasonable to expect that the presence of shells might influence the SBF signal of the galaxy. In this respect, the high quality of Advanced Camera for Surveys (ACS) images is crucial to remove the shell structure, allowing the measurement of SBF of the galaxy, even at high distances. Thus, the SBF measurement remains a relevant tool to investigate the distance of shell galaxies.

In the present work, we derive SBF magnitudes of a sample of distant shell ellipticals taking advantage of the high resolution power of the ACS on board of the *Hubble Space Telescope* (*HST*). We select deep ACS images and measure F814W-band ($\sim I$-band) SBF of the four galaxies: PGC 6510, PGC 10922, PGC 42871, and PGC 6240, with recession velocities reaching ≈ 8000 km s^{-1}. The main goal of our work is to measure their distance by using the SBF technique. No previous distance determination is available for any of these galaxies, except for the kinematic distance modulus. The farthest object of the sample, at a distance of $\sim$100 Mpc, lies near the upper limit of distances obtained using optical SBF measurements (Thomsen et al. 1997; Mei et al. 2003). It is worth noticing that none of these objects has been previously analyzed in detail, with the only exception of the recent work of Maybhate et al. (2007) on the globular cluster (GC) system of PGC 6240.

In the next section we present the observational data and the general properties of the selected galaxies. The procedure to derive the SBF measurements and the data analysis are described in § 3. The results are presented and discussed in § 4, where we provide new SBF predictions together with new calibrations of absolute SBF magnitudes for the *HST* ACS filters based on single-burst stellar population (SSP) models. In the same section,

[1] INAF– Osservatorio Astronomico di Teramo, Via M. Maggini s.n.c., I-64100 Teramo, Italy; biscardi@oa-teramo.inaf.it, raimondo@oa-teramo.inaf.it, cantiello@oa-teramo.inaf.it, brocato@oa-teramo.inaf.it.

[2] Dipartimento di Fisica, Università di Roma Tor Vergata, via della Ricerca Scientifica 1, 00133 Rome, Italy.

[3] Department of Physics and Astronomy, Washington State University, Pullman, WA 99164.

TABLE 1
PROPERTIES OF GALAXIES

Galaxy (1)	T (2)	R.A. (3)	Decl. (4)	v_{rec} (km s^{-1}) (5)	DM (6)	A_B (7)	A_{F814W} (8)	A_{F475W} (9)	F814W (10)	F475W (11)
PGC 6510	−3	26.591	−83.400	4650 ± 22	34.0 ± 0.2	0.588	0.246	0.492	2712	7874
PGC 10922	−2	43.400	−83.142	4825 ± 42	34.1 ± 0.2	0.370	0.156	0.312	3970	9350
PGC 42871	0	191.022	−34.202	6400 ± 36	34.7 ± 0.2	0.290	0.121	0.242	5908	8369
PGC 6240	−3	25.379	−65.615	7936[a] ± ...	35.2 ± 0.5	0.088	0.036	0.072	7300	21440

NOTES.—Col. (1): Galaxy name. Col. (2): Morphological T-type from RC3. Cols. (3) and (4): right ascension and declination from RC3 (J2000.0). Col. (5): Recession velocity in the CMB reference frame corrected for Virgo + Great Attractor + Shapley's infall (data from the NED database, http://nedwww.ipac.caltech.edu). Col. (6): Kinematic distance modulus obtained using $H_0 = 73 \pm 5$ km s^{-1} Mpc^{-1} (from NED). Col. (7): B-band extinction from Schlegel et al. (1998). Cols. (8) and (9): F814W- and F475W-band extinctions, calculated from A_B using Sirianni et al. (2005) coefficients. Cols. (10) and (11): Total exposure time for F814W and F475W images.
[a] For this galaxy only the Virgo infall corrected recession velocity is available.

an evaluation of H_0 is also obtained. A brief summary is given in § 5.

2. THE OBSERVATIONAL DATA

The *HST* images used in the present work were obtained with ACS in its Wide Field Channel mode. The large field of view, high resolution, and sharp point-spread function (PSF) characterizing ACS images are critical requirements to attempt the SBF measurements of the distant galaxies we have selected.

The images were retrieved from *HST* archive. A requirement in selecting the data is that the SBF S/N ratio in the F814W band is $\gtrsim$5, as suggested by Blakeslee et al. (1999). This condition is verified for the three ellipticals PGC 6510, PGC 10922, and PGC 42871, while PGC 6240 images have slightly lower S/N ($\approx$4). For these galaxies F475W images were also available, although the exposure times prevented their use to measure SBF (S/N $\ll$ 5). However, they were retrieved and analyzed to obtain integrated magnitudes and colors. The images are associated with proposal GO 10227 (PI: P. Goudfrooij) designed to study the globular cluster system of the four giants, poststarburst shell ellipticals. The main properties of the selected galaxies are reported in Table 1.

We downloaded the ACS images processed with the standard calibration pipeline (CALACS), that includes bias, dark, and flat-fielding corrections. The images from the archive still require the final image combination and the correction to remove the geometric distortions. To this purpose we used the PYRAF task `multidrizzle` (Koekemoer et al. 2002), that also provides the bad pixel identification and the cosmic-ray rejection. No sky subtraction was performed at this stage. To reduce the effect of noise correlation introduced by the drizzling procedure (Fruchter & Hook 2002), we adopted the LANCZOS3 kernel which, as demonstrated by Mei et al. (2005) and Cantiello et al. (2005) is adequate for the purpose of SBF estimation.

3. DATA ANALYSIS

To derive the SBF measurements we follow the same basic procedure adopted in Cantiello et al. (2005, 2007). In this section, we summarize the relevant steps to measure SBF magnitudes and we enlighten the differences from the quoted works.

First, a provisional sky value is derived from the corner with lowest sky counts, and a mask of the bright sources (saturated stars, extended galaxies, etc.) is obtained. Then, the brightness profile of the galaxy is modeled using the IRAF[4]/STSDAS task ELLIPSE (Jedrzejewski 1987). After the galaxy model is subtracted, we derive a new mask of the faint sources which clearly appears after the galaxy light is removed. This new mask is fed to ELLIPSE to obtain a new galaxy model.

We use the isophotal geometry, as derived with the last galaxy model, to get the surface brightness and color profiles of the galaxy. The galaxy profile is fit using a de Vaucouleurs law to find the sky as the zero-point constant in the fit. For all galaxies, we find that a de Vaucouleurs law is well suited in the 1″–5″ region of the galaxy. This result confirms the known evidence that the photometry of shell galaxies is the same expected for a normal elliptical (e.g., Wilkinson et al. 2000).

The new sky value is adopted and all the above steps are iterated, until convergence. At the end of these iterations we have the final sky value, the mask of external sources, and the best galaxy model. The final surface brightness and color profiles for the four galaxies are shown in Figure 1. It is worth noting that the average color of the four galaxies is bluer than in normal ellipticals, and the color gradient is positive or nearly flat. Both characteristics can be considered normal for this class of galaxies (Tamura et al. 2000; Lee et al. 2006). For all data we apply a K-correction $K_{F814W} \approx K_I \approx 0.5z$ and $K_{F475W} \approx K_g \approx 2z$ (Poggianti 1997) for integrated color. The extinction correction are evaluated using the prescriptions given by Sirianni et al. (2005, their Table 14).

We subtract the sky value and the galaxy model from the original image. This operation leaves a large-scale residual background, due to mismatch of the real galaxy with the model. The large-scale residuals are removed using the background map derived with the photometry package SExtractor (Bertin & Arnouts 1996). We have carried out some numerical experiments to determine the best background map parameters able to provide both a good subtraction of the large-scale residuals, and the best possible removal of the shell features. After several experiments we have chosen a mesh size of 15×15 pixels^2 (BACK_SIZE = 15), with three background-filtering meshes (BACK_FILTERSIZE = 3).

Up to this point, the procedure is applied to both filters. The sky, galaxy model, and large-scale residuals are subtracted to the original frame to derive the *residual* frame. Note that possible dust regions, as found in PGC 42871, are masked out since they could compromise the SBF measurement. Such regions are better recognized from the F475W image, the same dust mask is used for both filters.

We run SExtractor on the residual frame to obtain the photometric catalog of external sources (foreground stars, globular clusters and background galaxies). This photometric catalog is used to construct the luminosity functions (LFs), which will be used to estimate the contribution to the fluctuations coming from faint unmasked external sources (P_{res}).

[4] IRAF is distributed by the National Optical Astronomy Observatory, which is operated by the Association of Universities for Research in Astronomy, Inc., under cooperative agreement with the National Science Foundation.

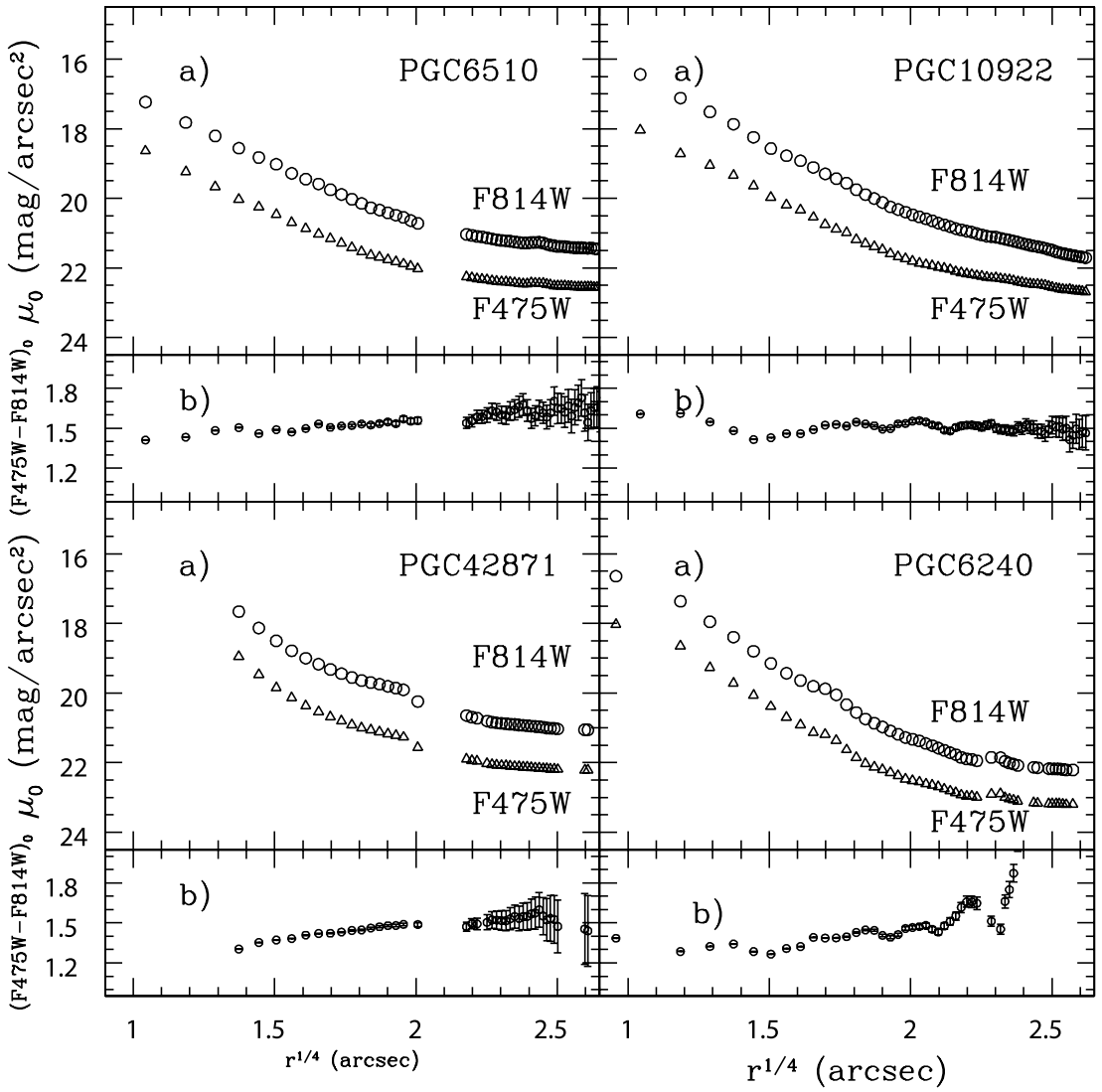

FIG. 1.—(*a*) F814W/F475W band surface brightness profile as function of $r^{1/4}$ (*open circles/triangles*). (*b*) Measured $(B-I)_0$ profile as function of $r^{1/4}$. Data are corrected for Galactic extinction and *K*-correction.

The procedures used to fit the LFs are the same described in Cantiello et al. (2005). In particular, we adopted $M_I = -8.5$ mag as the absolute turn-over magnitude (TOM) of the GCLF (Harris 2001), while the exponent for the power-law LF of background galaxies is $\gamma = 0.34$ (Bernstein et al. 2002). These parameters are used to start an iterative fitting process where the surface density of galaxies and globular clusters, and the galaxy distance are allowed to vary until their best values are found via a maximum likelihood method. Figure 2 shows the best fit of the observed LFs obtained for the four galaxies, used to derive $P_{\rm res}$.

Before computing the power spectra of the residual image and of the PSF, and evaluate their azimuthal averages, we mask regions with residual contamination from shells, and divide the residual frame by the square root of the galaxy model. It is worth noting here that only the shells not completely removed by the background map subtraction, i.e., the most prominent shells, required further masking.

The frames obtained with the analysis described up to this point are shown in Figure 3. We point out that in general the residuals appear similar to typical residual frames of SBF measurements of normal ellipticals. Nevertheless, in Figure 3 we adopted a scale to emphasize the regions where the procedure described failed in the complete subtraction of shells (in particular, PGC 42871 and PGC 6240). To quantify the additional systematic uncertainty due to unsubtracted shells, we performed a specific test described at the end of this section.

Next, the total fluctuation amplitude is determined as the constant factor P_0 multiplied by the PSF power spectrum, to match the power spectrum of the residual frame $P(k)$:

$$P(k) = P_0 E(k) + P_1, \tag{1}$$

where P_1 is the white-noise component, and $E(k)$ is the convolution between the PSF power spectrum and the power spectrum of the mask function. The latter mask also takes into account the shape of the galaxy annulus adopted for the SBF measurement. The minimum annular radius has been fixed to be the minimum radius without dust contamination, while the maximum radius is fixed to the region where the galaxy to sky counts ratio is $\gtrsim 1$.[5]

[5] As in Cantiello et al. (2007), we consider one single annulus per galaxy, because of the lower S/N ratio of the images, and because of the, on average, small available area. It must be noted that in our procedure the contribution of the external sources is evaluated taking into account their radial position, so that using one single annulus does not introduce any systematics on $P_{\rm res}$. Moreover, we have carried out a three-annuli measurement on the galaxy with the largest spatial extension, PGC 6510; as a result, we found that the averaged value agrees within uncertainties with the measurement reported in Table 2.

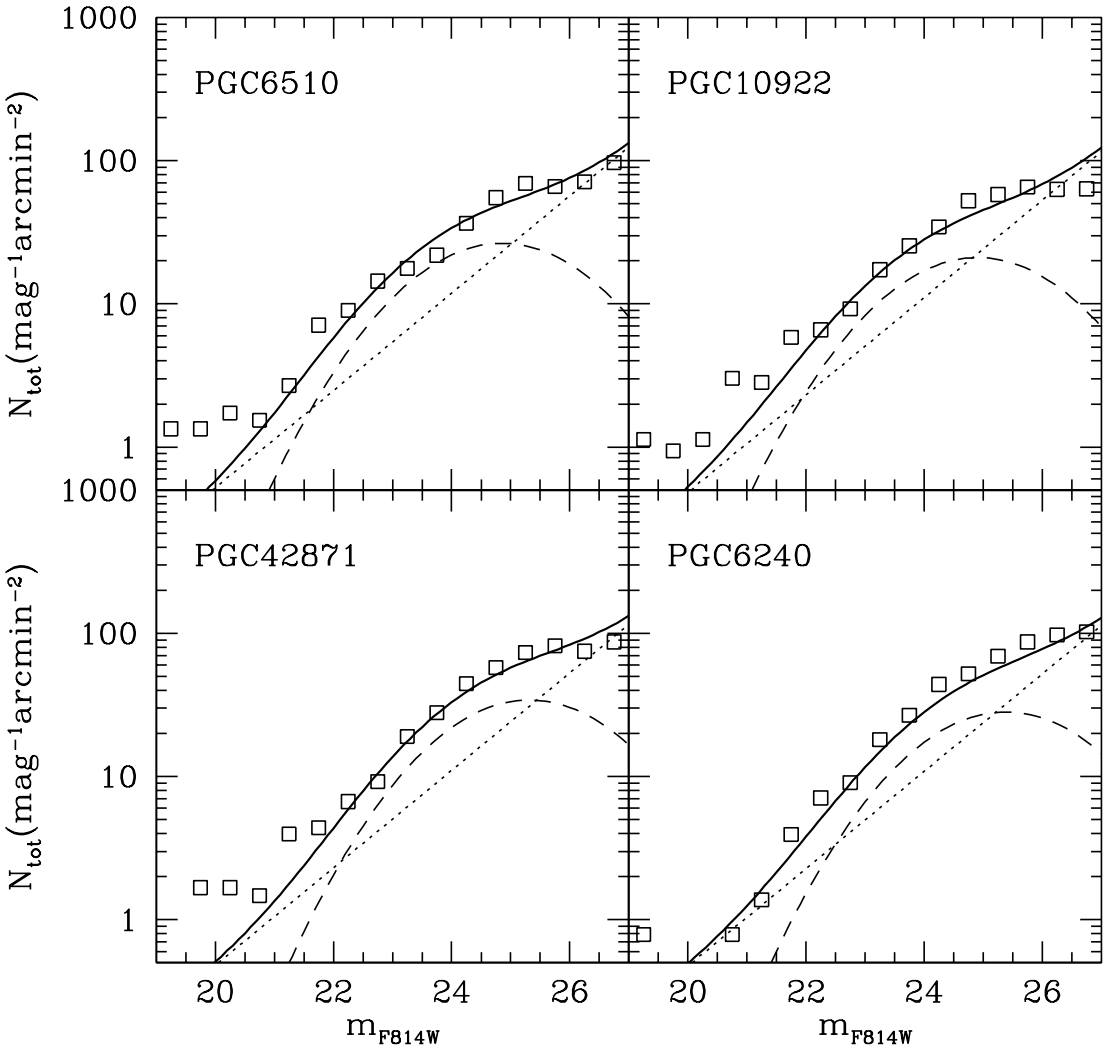

FIG. 2.—LFs of external sources. Open squares mark observational data; model fits to globular cluster and galaxy LFs are shown as dashed and dotted lines, respectively, and their sum as a solid line.

A robust linear least-squares method (Press et al. 1992) is used to fit equation (1). The lowest k-numbers ($k < 250$), that have been corrupted by the subtraction of the smooth background profile (Blakeslee et al. 1999), and the high k-numbers ($k > 600$), that have been corrupted by the drizzling procedure, are excluded from the fitting (see Cantiello et al. 2005 and 2007 for more details).

Figure 4 exhibits the azimuthal average of the power spectrum for each galaxy, the best fit lines are also shown.

Finally, the SBF magnitude is evaluated as

$$\overline{m}_{\rm F814W} = -2.5\log(P_0 - P_{\rm res}) + m^* - A_{\rm F814W} - K_{\overline{\rm F814W}}, \quad (2)$$

where $P_{\rm res}$ is the extra contribution of unmasked external sources, evaluated from the fitted LF as described in the quoted papers. The amplitude of $P_{\rm res}$ is small for all galaxies of the sample, being on average $P_{\rm res}/P_0 \sim 0.08$ (Table 2); m^* is the zero-point ACS magnitude in the VEGAMAG system reported by Sirianni et al. (2005; $m^*_{\rm F814W} = 25.501$ mag), $A_{\rm F814W}$ is the extinction correction in the F814W passband, and $K_{\overline{\rm F814W}}$ is the K-correction term. We apply $K_{\overline{\rm F814W}} \approx 7z$ after Thomsen et al. (1997).

We used Sirianni et al. (2005) equations to transform the F814W and F475W into the standard B and I magnitudes. However, in the forthcoming section we also take into account the magnitudes in the ACS photometric system.

The main differences between the present data and the images used by Cantiello et al. (2005, 2007) are (1) the much greater distance of the objects, which affects the LF fitting, and (2) the rather complex shell structure. For this reason we have performed two additional tests with respect to the ones described in the quoted papers.

The first one is related to the globular cluster LF (GCLF). The data quality of the images in some cases does not allow to reliably sample the TOM of the GCLF. This is confirmed by the recent work published by Maybhate et al. (2007) on the GCLF of PGC 6240, based on the same data used here. These authors do not provide an estimation of the TOM, however, from a visual inspection of their Figure 11, the extrapolated TOM appears $\approx$1 mag fainter than the one adopted here. Since the large uncertainty, we perform a specific test to evaluate its effect on the SBF. Adopting the GCLF of Maybhate et al., the SBF magnitude changes a few hundredths of mag ($\lesssim$0.05 mag), that is a $\sim$3% uncertainty on the distance.

The second test concerns how the presence of shells affects SBF. To evaluate this effect we selected the farthest galaxy in the sample (PGC 6240), then we run the whole SBF measurement

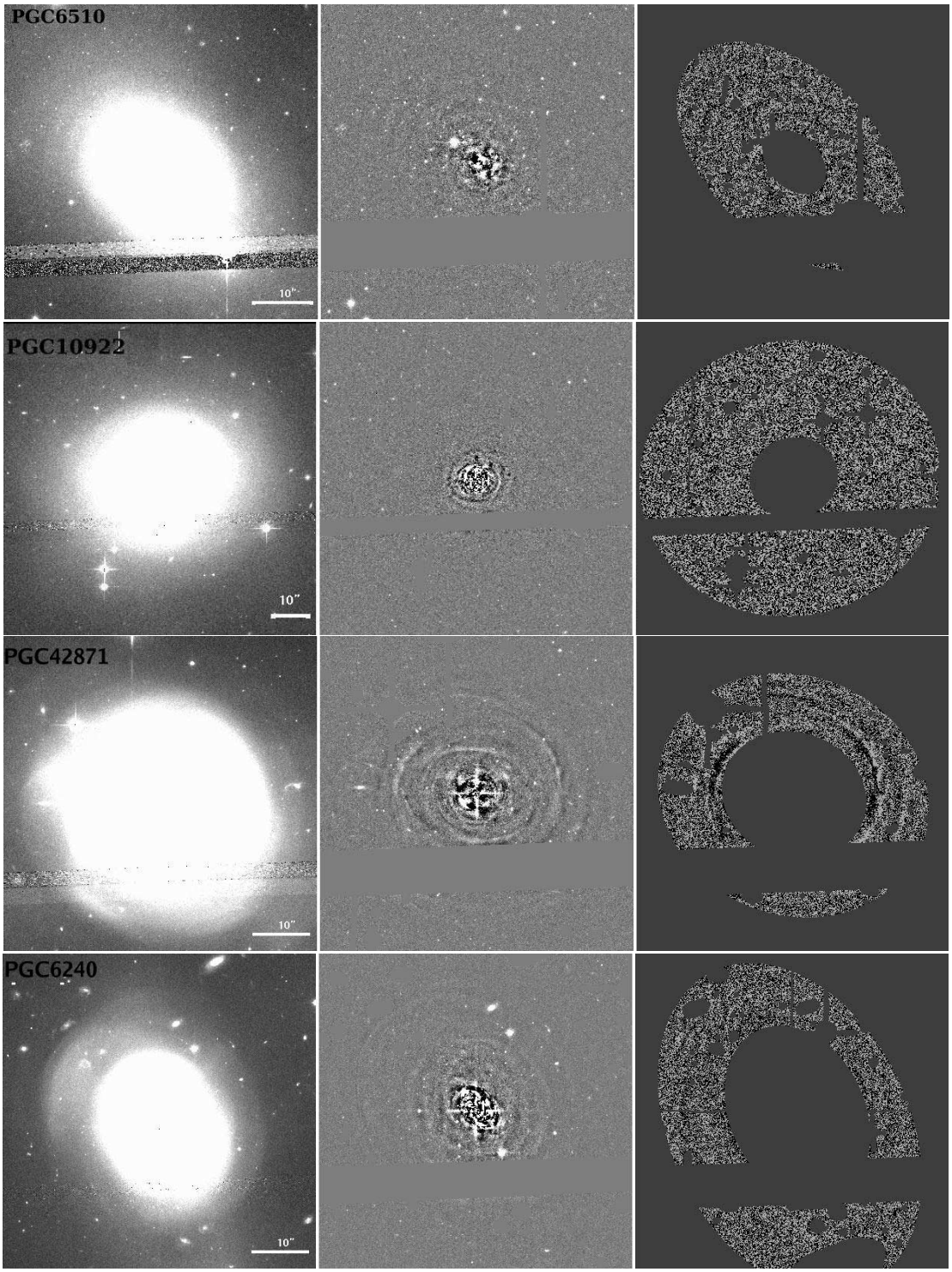

FIG. 3.—*From left to right*: The original *I*-band frame, residual frame, and residuals times of the final adopted mask, for each galaxy (*upper left label in each panel*).

procedure on the image, with and without masking the most prominent shell. The result of this test shows that the final SBF magnitude changes by $\lesssim$0.25 mag. Even though this is not an exhaustive evaluation of the uncertainty caused by shell features, it is a robust suggestion that the adopted procedure should keep this source of uncertainty fairly below 0.25 mag. Thus, we consider this value as the upper limit of systematic uncertainties due to possible unmasked residual shells.

In conclusion, the total statistical uncertainty on the SBF is obtained as the square sum of the fitting uncertainty on P_0, and the default 25% uncertainty on $P_{\rm res}$ (Tonry et al. 1990). The effect of the sky uncertainty is negligible on the SBF, while it is the main source of error in the color. In addition, these measurements suffer for a total systematic uncertainty due to (1) the PSF normalization ($\approx$0.03 mag), (2) the fit of LFs ($\approx$0.05 mag), (3) the filter zero points ($\approx$0.01 mag), and (4) if necessary, the transformation from the ACS photometric system to the standard system ($\approx$0.02 mag). Summing in quadrature all the systematic sources of errors, we find that a total systematic uncertainty $\approx$0.1 mag affects our SBF measurements (Cantiello et al. 2005).

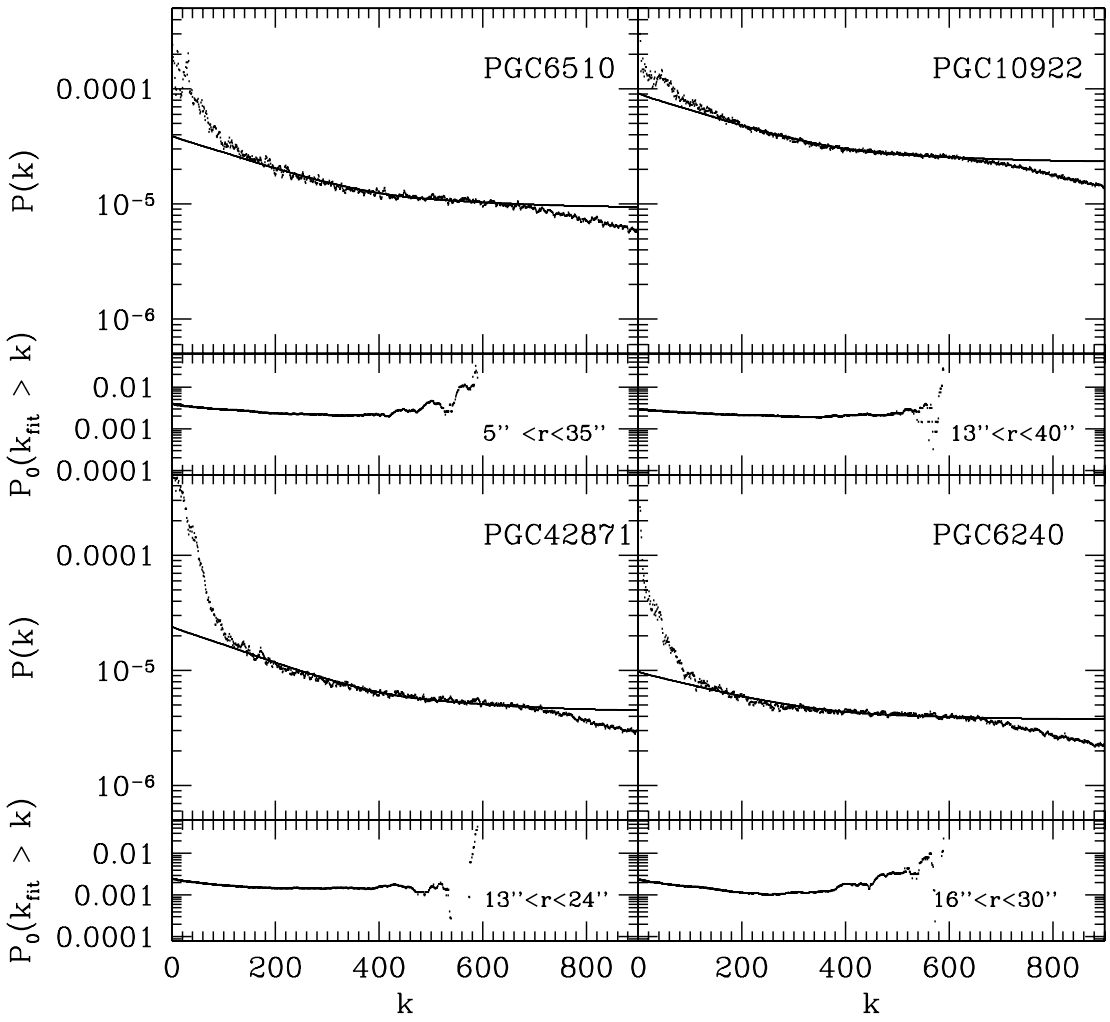

FIG. 4.—For each labeled galaxy, the top panels show the azimuthal average of the power spectrum (the average radii of the annuli used are reported in each panel). The observational data (*dots*) are fitted by the sum of a scaled PSF power spectrum plus the constant white-noise term (*solid line*). The lower panels show the P_0 obtained as a function of the starting wavenumber of the fit, $P_0(k_{fit} > k)$. The final P_0 adopted is the weighted average of values in the flatter P_0 vs. k-region. We excluded the lowest k-numbers, that have been corrupted by the background subtraction, and the highest k-numbers, that have been corrupted by the drizzling procedure.

On average, this corresponds to a systematic error of ≈6% on distances and on the Hubble constant. If we also add the maximum systematic uncertainty of ≈0.25 mag due to the presence of shells, the total systematic error becomes ≈12%. It is worth emphasizing here, again, that the 0.25 mag systematic uncertainty due to the shells is an upper limit, as it has been derived from the worst case, i.e., farthest galaxy, prominent shells.

Table 2 reports the final SBF measurements and statistical uncertainties for all galaxies. In the table we also report the SBF and colors obtained transforming the ACS filters F475W and F814W into standard B and I passbands.

4. DISCUSSION

4.1. *Calibration, SBF Models, and Distances*

The application of SBF method as distance indicator requires the calibration of the absolute SBF magnitude, $\overline{M}$, versus the broadband color. To date, no calibration is available for the ACS

TABLE 2
COLOR AND SBF MEASUREMENTS

Galaxy (1)	Annulus (arcsec) (2)	P_0 (ADU s^{-1}) (3)	P_{res} (ADU s^{-1}) (4)	$\overline{m}_{F814W,0}$ (mag) (5)	$(F475W - F814W)_0$ (mag) (6)	$\overline{m}_{I,0}$ (mag) (7)	$(B - I)_0$ (mag) (8)
PGC 6510	6–35	0.0031 ± 0.0001	0.0002	31.65 ± 0.04	1.47 ± 0.05	31.70 ± 0.04	1.86 ± 0.05
PGC 10922	13–40	0.00225 ± 0.00004	0.0002	31.93 ± 0.04	1.42 ± 0.04	31.97 ± 0.04	1.79 ± 0.04
PGC 42871	13–24	0.0045 ± 0.0002	0.0005	32.18 ± 0.04	1.35 ± 0.03	32.22 ± 0.08	1.70 ± 0.03
PGC 6240	16–30	0.00125 ± 0.00006	0.0001	32.63 ± 0.06	1.23 ± 0.03	32.68 ± 0.06	1.57 ± 0.03

NOTES.—The magnitudes are extinction and K-corrected. Col. (1): Galaxy name. Col. (2): Average annulus inner-outer radii for SBF measurements. Col. (3): Average P_0. Col. (4): Unmasked external sources fluctuation contribution P_{res}. Col. (5): SBF magnitude. Col. (6): $(F475W - F814W)_0$ color. Col. (7): SBF magnitude in the standard photometric system. Col. (8): $(B - I)_0$ integrated color.

TABLE 3
SBF Models

Age (Gyr) (1)	$\overline{F435W}$ (mag) (2)	$\overline{F475W}$ (mag) (3)	$\overline{F550M}$ (mag) (4)	$\overline{F555W}$ (mag) (5)	$\overline{F606W}$ (mag) (6)	$\overline{F625W}$ (mag) (7)	$\overline{F775W}$ (mag) (8)	$\overline{F814W}$ (mag) (9)	$\overline{F850LP}$ (mag) (10)	$(F475W - F814W)_0$ (mag) (11)
					$Z = 0.008$					
1.5.....	1.988	1.201	−.021	0.277	−.361	−.766	−2.075	−2.387	−3.090	1.298
2.0.....	2.097	1.287	0.086	0.376	−.249	−.642	−1.959	−2.277	−2.987	1.395
3.0.....	2.167	1.363	0.200	0.479	−.129	−.510	−1.871	−2.203	−2.928	1.501
4.0.....	2.332	1.532	0.382	0.658	0.055	−.322	−1.708	−2.050	−2.793	1.504
5.0.....	2.242	1.465	0.353	0.619	0.038	−.328	−1.645	−1.973	−2.696	1.575
7.0.....	2.264	1.475	0.368	0.632	0.050	−.312	−1.711	−2.061	−2.809	1.621
9.0.....	2.429	1.664	0.587	0.843	0.277	−.079	−1.450	−1.805	−2.569	1.656
11.0.....	2.380	1.636	0.587	0.835	0.284	−.064	−1.433	−1.805	−2.601	1.694
13.0.....	2.431	1.698	0.658	0.905	0.354	0.008	−1.398	−1.776	−2.579	1.72
14.0.....	2.393	1.668	0.639	0.883	0.337	−.007	−1.412	−1.795	−2.605	1.737
					$Z = 0.01$					
1.5.....	2.094	1.323	0.113	0.412	−.230	−.634	−2.014	−2.347	−3.086	1.309
2.0.....	2.270	1.471	0.271	0.563	−.065	−.460	−1.835	−2.177	−2.935	1.42
3.0.....	2.402	1.594	0.414	0.701	0.080	−.305	−1.732	−2.094	−2.879	1.528
4.0.....	2.489	1.690	0.527	0.810	0.196	−.185	−1.657	−2.039	−2.854	1.573
5.0.....	2.304	1.506	0.368	0.643	0.048	−.322	−1.712	−2.074	−2.862	1.612
7.0.....	2.350	1.572	0.468	0.734	0.154	−.206	−1.608	−1.983	−2.783	1.648
9.0.....	2.470	1.707	0.630	0.888	0.325	−.029	−1.394	−1.771	−2.584	1.687
11.0.....	2.465	1.701	0.626	0.883	0.317	−.036	−1.427	−1.807	−2.621	1.725
13.0.....	2.477	1.737	0.690	0.940	0.389	0.042	−1.346	−1.739	−2.581	1.753
14.0.....	2.572	1.833	0.782	1.034	0.477	0.129	−1.289	−1.694	−2.553	1.766
					$Z = 0.02$					
1.5.....	2.579	1.848	0.647	0.956	0.311	−.091	−1.582	−1.994	−2.903	1.431
2.0.....	2.723	1.933	0.708	1.018	0.369	−.030	−1.478	−1.889	−2.816	1.524
3.0.....	2.903	2.096	0.874	1.183	0.539	0.145	−1.352	−1.786	−2.734	1.615
4.0.....	2.926	2.139	0.964	1.260	0.642	0.262	−1.185	−1.628	−2.606	1.673
5.0.....	2.803	2.006	0.832	1.126	0.513	0.137	−1.283	−1.704	−2.629	1.703
7.0.....	2.912	2.121	0.974	1.259	0.662	0.294	−1.074	−1.489	−2.415	1.749
9.0.....	3.003	2.229	1.108	1.385	0.800	0.438	−.906	−1.320	−2.260	1.793
11.0.....	2.981	2.204	1.080	1.357	0.769	0.407	−.910	−1.324	−2.271	1.826
13.0.....	2.992	2.230	1.123	1.396	0.814	0.455	−.901	−1.337	−2.322	1.862
14.0.....	2.979	2.230	1.147	1.413	0.845	0.493	−.820	−1.248	−2.227	1.876
					$Z = 0.04$					
1.5.....	2.903	2.198	1.035	1.340	0.734	0.350	−1.135	−1.619	−2.699	1.533
2.0.....	3.057	2.318	1.146	1.450	0.845	0.465	−.999	−1.482	−2.564	1.604
3.0.....	3.308	2.545	1.373	1.674	1.073	0.696	−.744	−1.248	−2.390	1.691
4.0.....	3.428	2.659	1.489	1.789	1.192	0.819	−.614	−1.121	−2.277	1.743
5.0.....	3.073	2.303	1.152	1.444	0.863	0.499	−.819	−1.269	−2.318	1.785
7.0.....	3.245	2.453	1.295	1.587	1.005	0.643	−.701	−1.171	−2.247	1.846
9.0.....	3.273	2.494	1.360	1.645	1.073	0.717	−.600	−1.059	−2.132	1.886
11.0.....	3.315	2.552	1.442	1.719	1.160	0.809	−.443	−.890	−1.968	1.922
13.0.....	3.405	2.650	1.549	1.824	1.266	0.917	−.330	−.772	−1.842	1.955
14.0.....	3.281	2.529	1.438	1.709	1.157	0.811	−.449	−.902	−1.990	1.97

Note.—Col. (1): Age. Cols. (2)–(10): Absolute SBF magnitudes in various ACS photometric filters. Col. (11): $(F475W - F814W)_0$ integrated color.

F814W bandpass versus $(F475W - F814W)_0$ color, in the color range of the present galaxies sample. Moreover, even transforming the $(F475W - F814W)_0$ color to the standard $(B - I)_0$ color, the empirical calibration of SBF in the standard I band determined by Cantiello et al. (2005) is defined in the color range $2.0 \leq (B - I)_0 \leq 2.25$, while all our galaxies have $(B - I)_0 \leq 2.0$ mag. Thus, we decided to extend to bluer colors the calibration of absolute SBF magnitudes, by using models.

The SBF models used here are based on the most updated version of the code SPoT (Stellar Population Tools; Raimondo et al. 2005).[6] These models have the advantage of fitting the SBF and color of ellipticals, as well as of resolved and unresolved stellar clusters, for a wide range of ages and metallicities (see Raimondo et al. and references therein for details). For the specific purpose of this study, we computed the theoretical SBFs in the ACS VEGAMAG photometric system using the BaSeL 3.1 (Westera et al. 2002; Patricelli 2006) stellar atmospheres library. The resulting SBF magnitudes are reported in Table 3.

[6] See http://www.oa-teramo.inaf.it/SPoT.

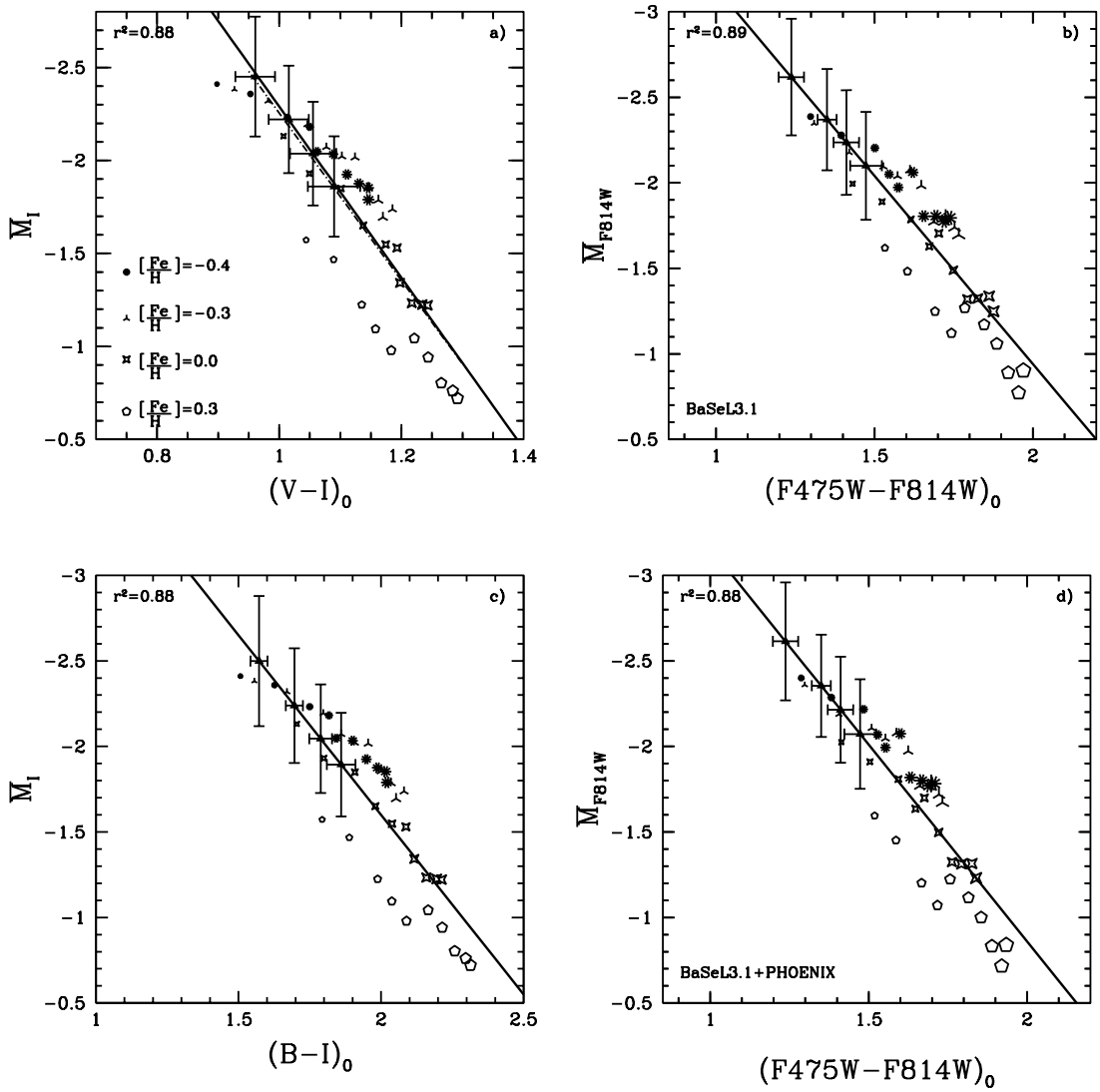

FIG. 5.—Absolute SBF magnitudes vs. integrated colors. In the figure we plot our models of different metallicities (as labeled) and ages ($t = 1.5, 2, 3, 4, 5, 7, 9, 11, 13$, and 14 Gyr). Symbols with increasing size mark models of older age. Filled triangles mark the observational data. In each panel we report the linear fit to models (*solid line*) and the correlation coefficient r^2 (*top left label*). (*a*) The calibration of $\overline{M}_I$ vs. $(V-I)_0$ from Jensen et al. (2003) is shown with a dot-dashed line. (*b*) Same as (*a*), but the absolute $\overline{M}_{\rm F814W}$ magnitude and $({\rm F475W}-{\rm F814W})_0$ color are used. (*c*) Same as (*a*), but the $(B-I)_0$ color is used. (*d*) Same as (*b*), but a different stellar atmosphere library is used (*bottom left label*).

We start with the empirical calibration by Jensen et al. (2003):

$$\overline{M}_I = (-1.58 \pm 0.08) + (4.5 \pm 0.25) \times [(V-I)_0 - 1.15], \quad (3)$$

defined in the color range $0.95 \leq (V-I)_0 \leq 1.3$. This relation has a high degree of reliability, since the zero-point magnitude has been obtained using the improved period-luminosity relations for Cepheids by Udalski et al. (1999) and the slope is the one derived by Tonry et al. (1997) based on group membership of galaxies. On the theoretical side, we fit the SBF versus color models with a robust straight line fitting process that minimizes the mean absolute deviation. We selected stellar population models in the age range $1.5 \leq t({\rm Gyr}) \leq 14$, and the metallicity range $-0.4 \leq [{\rm Fe/H}] \leq 0.3$ (Fig. 5*a*). As a result we obtain

$$\overline{M}_I = (-1.6 \pm 0.1) + (4.5 \pm 0.2) \times [(V-I)_0 - 1.15], \quad (4)$$

in very good agreement with equation (3).

The same models, but for the ACS photometric system, are compared to the observational data from the ACS Virgo Cluster Survey (Mei et al. 2007). We have adopted a DM $\simeq 31.1$ for the Virgo Cluster (Ferrarese et al. 2000), and transformed models into the ABMAG photometric system for sake of homogeneity with data (Fig. 6). A linear fit to models provides a slope $\alpha = 1.4 \pm 0.1$ and intercept $\beta = 29.0 \pm 0.1$, in good agreement with the empirical fits provided by Mei and collaborators, who give $\alpha = 1.3 \pm 0.1$ and $\beta = 29.09 \pm 0.04$. We have also checked the case of a double linear fit, as suggested by the authors. We obtained $\alpha = 0.8 \pm 0.1$ and $\beta = 29.0 \pm 0.1$ in the color interval $1.0 \leq ({\rm F475W}-{\rm F850LP})_0 \leq 1.3$, while $\alpha = 1.7 \pm 0.1$ and $\beta = 29.0 \pm 0.1$ in the color range $1.3 < ({\rm F475W}-{\rm F850LP})_0 \leq 1.6$. In both cases the fit from models agrees within 1 σ with the empirical calibrations.

Before going further, we evaluate the capability of the SBF method to derive accurate distances of shell ellipticals, as their peculiar morphology might disturb the SBF measurement. To this purpose, we selected a sample of shell galaxies from the Tonry et al. (2001) database, for which the distance modulus (DM) is available from methods not related to the SBF technique (Table 4). The absolute SBF magnitudes, $\bar{M}_{\text{non-SBF DMs}}$, of these

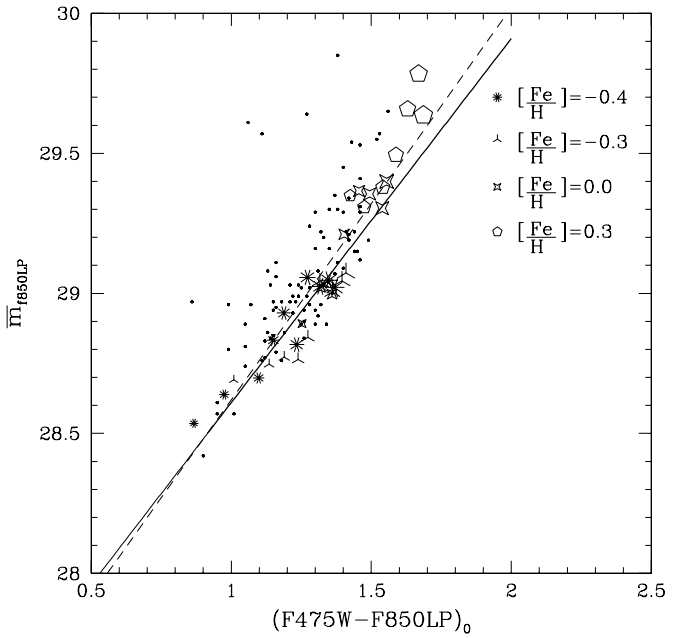

FIG. 6.—Plot of $\overline{m}_{F850LP}$ vs. $(F475W - F850LP)_0$. In the figure we plot the new SBF models in the ACS photometric system (ABMAG), shifted to a Virgo distance modulus of 31.1 (symbols are as in Fig. 5). The observational data (*filled dots*) are from Mei et al. (2007). The best fit of the present SBF models is shown as a solid line, the best fit of the data by Mei et al. (2007) is reported as a dashed line.

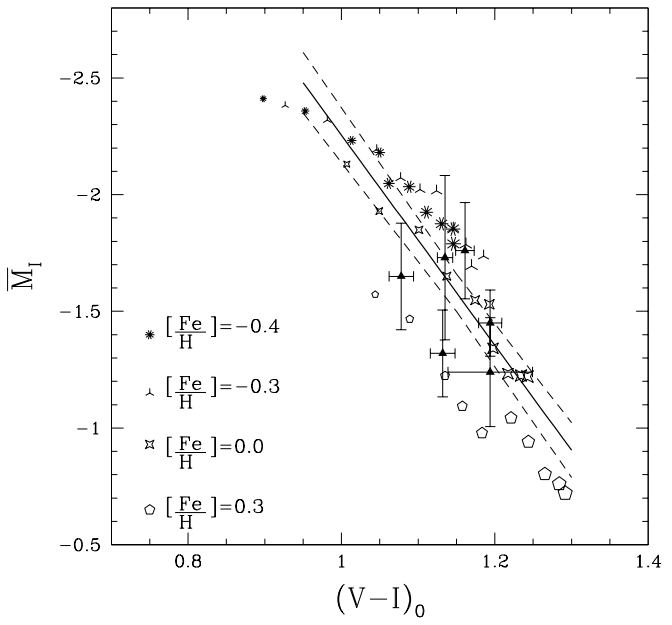

FIG. 7.—$\overline{M}_I$ vs. $(V - I)_0$. Symbols are as in Fig. 5. In the figure we plot the calibration from Jensen et al. (2003; *solid line*), and 1 σ dispersion lines are reported with the dashed line. A sample of shell elliptical galaxies from Tonry et al. (2001) are reported as triangles. The absolute SBF magnitudes are derived coupling the apparent SBF measurements, with the SBF-independent DMs reported in Table 4. It is noticeable the absence of any systematic deviation of shell ellipticals with respect to the empirical calibration ($\langle \bar{M}_{J03} - \bar{M}_{\text{non-SBF DMs}} \rangle = -0.06 \pm 0.22$), and to the stellar population models.

shell galaxies, calculated as the difference between the SBF apparent magnitude, $\bar{m}_{T01}$, and the non-SBF DMs listed in Table 4, are reported in Figure 7. The solid line in the figure represents the empirical calibration, equation (3), from Jensen et al. (2003). Taking into account the uncertainties, the observational data are consistent with the empirical calibration. The median difference between the absolute SBF magnitude predicted using equation (3) and $\bar{M}_{\text{non-SBF DMs}}$ is $\langle \bar{M}_{J03} - \bar{M}_{\text{non-SBF DMs}} \rangle = -0.06 \pm 0.22$ mag, so that no systematic offset is recognized. Moreover, the datapoint nicely overlap with models. These results provide a further support in using the SBF method to derive distances of shell ellipticals.

Relying on these agreements, and using the same set of stellar population models matching the Jensen et al. (2003) equation, we derived

$$\overline{M}_{F814W} = (-0.94 \pm 0.20) + (2.2 \pm 0.2) \times [(F475W - F814W)_0 - 2.0], \quad (5)$$

the relation is shown in Figure 5*b*.

Following the same procedure, we derived the $\overline{M}_I$ versus $(B\text{-}I)_0$ calibration (see Fig. 5*c*), which extends to colors $(B - I)_0 \leq 2.0$ the previous calibration from Cantiello et al. (2005). The fit to models provides

$$\overline{M}_I = (-1.6 \pm 0.2) + (2.1 \pm 0.2)[(B - I)_0 - 2.0]. \quad (6)$$

Using equations (5) and (6) and the data in Table 2, we obtained the DMs reported in Table 5 (cols. [2] and [3]).

We note that the latter two relations may suffer of systematic uncertainties which typically affect stellar population synthesis models as, for example, the adopted library of stellar atmosphere models, especially for cool and bright stars. In Figure 5*d* we show the changes expected if a different stellar atmospheres library is used to obtain stellar population models in the F475W and F814W filters. The new atmospheres library is the combination of stellar models by Westera et al. (2002) for relatively hot stars ($T_e > 4500$ K), and by the PHOENIX models for cool stars

TABLE 4
NON-SBF DMs OF SHELL GALAXIES AND SBF MAGNITUDES FROM TONRY ET AL. (2001)

Galaxy (1)	$\bar{m}_{T01}$(mag) (2)	DM (mag) (3)	Distance Indicator (4)	Reference (5)
NGC 1316.....	29.83	31.2 ± 0.1	PNLF[a]	Ferrarese et al. (2000)
NGC 1344.....	29.67	31.4 ± 0.2	PNLF	Teodorescu et al. (2005)
NGC 3923.....	30.26	31.5 ± 0.2	GCLF	Sikkema et al. (2007)
NGC 4278.....	29.34	31.1 ± 0.1	GCLF	Kundu & Whitmore (2001)
NGC 5128.....	26.05	27.7 ± 0.2	Cepheids	Ferrarese et al. (2007)
NGC 4552.....	29.39	30.84 ± 0.09	GCLF	Kundu & Whitmore (2001)

NOTES.—Col. (1): Galaxy name. Col. (2): Apparent SBF magnitude measured by Tonry et al. (2001), corrected for extinction. Col (3): DM obtained from the distance indicator listed in col. (4). Col. (4): Reference for the DM.
[a] Planetary nebula LF.

TABLE 5
DISTANCE MODULI

Galaxy (1)	DM_{ACS}[a] (2)	$DM_{STD,\ BI}$[a] (3)	$DM_{STD,\ Jensen}$[a] (4)
PGC 6510	33.7 ± 0.25	33.6 ± 0.25	33.6 ± 0.15
PGC 10922	34.2 ± 0.25	34.1 ± 0.25	34.0 ± 0.15
PGC 42871	34.7 ± 0.25	34.6 ± 0.25	34.5 ± 0.15
PGC 6240	35.2 ± 0.25	35.2 ± 0.25	35.1 ± 0.2

NOTES.—Col. (1): Galaxy name. Col. (2): DM obtained with eq. (5). Col. (3): DM obtained with eq. (6). Col. (4): DM obtained with eq. (3).

[a] Statistical uncertainties are reported. The systematic error is ∼0.1 mag (see text).

(Brott & Hauschildt 2005). Adopting these atmosphere models, equation (5) becomes

$$\overline{M}_{\rm F814W} = (-0.86 \pm 0.20) + (2.3 \pm 0.2) \times [({\rm F475W} - {\rm F814W})_0 - 2.0].$$

The distance moduli obtained using the latter equation agree within uncertainties with those reported in Table 5. On average we find that the new DM varies less than 0.05 mag.

After transforming the $(B-I)_0$ colors in Table 2 to $(V-I)_0$ color, we also derived the distance moduli of the four galaxies using the empirical calibration, equation (3) and the $\bar{m}_I$ data in the Table 2. To this purpose, similarly to Cantiello et al. (2005) we derived the $(V-I)_0$ versus $(B-I)_0$ color transformation, using the same set of models adopted to obtain the equations (4)–(6). By fitting a straight line to the models, we derived

$$(V-I)_{0,\ {\rm transf}} = 0.47 \pm 0.02 \times (B-I)_0 + (0.21 \pm 0.02).$$

The distance moduli obtained from this procedure are in column (4) of Table 5. All the DMs from the different calibrations are in good agreement within uncertainties.

The uncertainties reported in Table 5 come from the propagation of statistical uncertainties already described in § 3, and from the calibrations uncertainty. In addition, the following systematic uncertainties should also be taken into account: (1) ∼0.1 mag from flat-fielding, filter zero point, etc., and, (2) the upper limit ∼0.25 mag, which is the maximum uncertainty possible due to possible residual shells.

Finally, we compare our distances with the ones obtained using the Hubble law, reported in Table 1. The recession velocity adopted for each galaxy are corrected for the Virgo + Great Attractor + Shapley supercluster infall, based on the local velocity field model given in Mould et al. (2000). The good matching of our DMs with the kinematic DMs ($\langle |{\rm DM_{SBF}} - {\rm DM}_{H_0}| \rangle < 0.2$) confirms that it is possible to measure reliable SBF magnitudes for galaxies up to 100 Mpc, even in the optical bandpasses, with an uncertainty of ±8 Mpc (statistical) ±6 Mpc (systematic, ±10 Mpc if the upper limit uncertainty due to possible unremoved shells is taken into account).

4.2. H_0 Determination

Since our galaxies are located beyond 4000 km s^{-1}, they constitute a good sample to determine the Hubble constant, H_0, given that the effect of local deviation from the smooth Hubble flow is minimized at this redshift. Using the distances based on the calibration equation (5), we estimate $H_0 = 76 \pm 6$ (statistical) ±5 (systematic; ±8 systematic including the upper limit uncertainty from possible unsubtracted shells) km s^{-1} Mpc^{-1}. It should be noted here that the H_0 value reported has been derived adopting the SBF measurements and the theoretical calibrations presented in this work; i.e., it does not suffer for the uncertainty of the Cepheids calibration. On the other hand, the adopted calibration suffers for the uncertainties and assumptions that are typically embedded in stellar population synthesis models (see, e.g., Charlot et al. 1996). However, the reliability of the present models is tested against known observational data (for example the empirical calibration from Jensen et al.). Such comparisons suggest that the theoretical systematic uncertainties are not larger than the quoted uncertainties.

Even if this determination is based on only four galaxies, it is interesting to note that the H_0 value derived is in good agreement with the final result from the *HST* Key Project Team, $H_0 = 72 \pm 4$ (statistical) ±8 (systematic) km s^{-1} Mpc^{-1}, and with the value $H_0 = 70 \pm 5$ (statistical) ±6 (systematic) km s^{-1} Mpc^{-1} obtained by the same authors using only SBF distances (Freedman et al. 2001). Finally, such value also agrees with the recent values $H_0 = 73 \pm 4$ (statistical) ±5 (systematic) km s^{-1} Mpc^{-1} determined by Riess et al. (2005) using the multicolor light curve shape method on two SNe Ia, and $H_0 = 72 \pm 4$ (statistical) ±4 (systematic) km s^{-1} Mpc^{-1} determined by Wang et al. (2006) obtained by using a sample of 109 SNe Ia and the ΔC_{12} method.

5. SUMMARY AND CONCLUSION

We presented F814W SBF measurements from ACS images of four distant shell elliptical galaxies with radial velocities between 4000 and 8000 km s^{-1}. By using the SBF method, the distance moduli of these galaxies are derived for the first time. We provided new calibration relations of the absolute SBF magnitude versus the integrated color, specifically the $\overline{M}_{\rm F814W}$ versus $({\rm F475W} - {\rm F814W})_0$. Moreover, the $\overline{M}_I$ versus $(B-I)_0$ relation presented here extends to bluer colors the calibration of Cantiello et al. (2005). The calibrations are based on new SBF models computed with the SPoT code for the ACS and standard filters. These models are aimed to simulate single-burst stellar populations of age ranging from $t = 1.5$ Gyr up to $t = 14$ Gyr and metallicity from $Z = 0.008$ to $Z = 0.04$. The use of a theoretical calibration is important not only because it is free from the uncertainties affecting empirical secondary distance indicators, but also because no empirical calibration of SBF magnitudes for these photometric bands is available in literature. To verify the reliability of the $\overline{M}_{\rm F814W}$ versus $({\rm F475W} - {\rm F814W})_0$ calibration we used exactly the same set of models to derive SBF-color relations in bands for which well established empirical calibrations are available (e.g., Jensen et al. 2003; Mei et al. 2007). As a result, the comparison between theoretical and empirical calibrations shows an extremely good agreement. This result added to positive tests already performed on resolved and unresolved stellar populations (e.g., Brocato et al. 1999, 2000; Cantiello et al. 2003; Raimondo et al. 2005; Fagiolini et al. 2007) makes us confident that the theoretical calibration presented here can be safely adopted to derive distances.

On the observational side, our measurements suffer for ∼0.1 mag systematic uncertainty in the SBF measurements coming from the filter zero point, flat-fielding, and PSF normalization. In addition, the presence of possible unsubtracted shells can affect the estimation of SBF amplitudes; we estimated an upper limit uncertainty of ∼0.25 mag from the worst case in the present data (PGC 6240: the farthest galaxy, prominent shell).

Coupling the SBF measurements with the theoretical calibrations we find distances in agreement with the ones obtained

using the Hubble law. The present measurements enlarge the sample of galaxies beyond 100 Mpc with optical SBF distances.

Finally, using our SBF distances, we derive $H_0 = 76 \pm 6$ (statistical) ± 5 (systematic; ± 8 systematic when the upper limit uncertainty from possible unsubtracted shells is included) km s^{-1} Mpc^{-1}, in good agreement with the most recent estimations of the Hubble constant.

It is a pleasure to acknowledge B. Patricelli for making available the color-temperature transformation for the ACS filters computed for her *Laurea* thesis. We also thank the referee for her/his useful suggestions which improved the paper. Financial support for this work was provided by PRIN-INAF 2006 "From Local to Cosmological Distances" (PI: G. Clementini).

REFERENCES

Ajhar, E. A., Blakeslee, J. P., & Tonry, J. L. 1994, AJ, 108, 2087
Bernstein, R. A., Freedman, W. L., & Madore, B. F. 2002, ApJ, 571, 107
Bertin, E., & Arnouts, S. 1996, A&AS, 117, 393
Blakeslee, J. P., Ajhar, E. A., & Tonry, J. L. 1999, in Post-*Hipparcos* Cosmic Candles, ed. A. Heck & F. Caputo (Dordrecht: Kluwer), 181
Brocato, E., Castellani, V., Poli, F. M., & Raimondo, G. 2000, A&AS, 146, 91
Brocato, E., Castellani, V., Raimondo, G., & Romaniello, M. 1999, A&AS, 136, 65
Brott, I., & Hauschildt, P. H. 2005, in The Three-dimensional Universe with *Gaia*, ed. C. Turon, K. S. O'Flaherty, & M. A. C. Perryman (ESA SP-576: Noordwijk: EAS), 565
Cantiello, M., Blakeslee, J. P., Raimondo, G., Mei, S., Brocato, E., & Capaccioli, M. 2005, ApJ, 634, 239
Cantiello, M., Raimondo, G., Brocato, E., & Capaccioli, M. 2003, AJ, 125, 2783
———. 2007, ApJ, 662, 940
Charlot, S., Worthey, G., & Bressan, A. 1996, ApJ, 457, 625
Fagiolini, M., Raimondo, G., & Degl'Innocenti, S. 2007, A&A, 462, 107
Ferrarese, L., et al. 2000, ApJ, 529, 745
Ferrarese, L., Mould, J. R., Stetson, P. B., Tonry, J. L., Blakeslee, J. P., & Ajhar, E. A. 2007, ApJ, 654, 186
Forbes, D. A., Reitzel, D. B., & Williger, G. M. 1995, AJ, 109, 1576
Freedman, W. L., et al. 2001, ApJ, 553, 47
Fruchter, A. S., & Hook, R. N. 2002, PASP, 114, 144
González, R. A., Liu, M. C., & Bruzual, A., G. 2004, ApJ, 611, 270
Harris, W. E. 2001, in Star Clusters, ed. L. Labhardt & B. Binggeli (Berlin: Springer), 223
Jedrzejewski, R. I. 1987, MNRAS, 226, 747
Jensen, J. B., Tonry, J. L., Barris, B. J., Thompson, R. I., Liu, M. C., Rieke, M. J., Ajhar, E. A., & Blakeslee, J. P. 2003, ApJ, 583, 712
Jensen, J. B., Tonry, J. L., Thompson, R. I., Ajhar, E. A., Lauer, T. R., Rieke, M. J., Postman, M., & Liu, M. C. 2001, ApJ, 550, 503
Jerjen, H., Binggeli, B., & Freeman, K. C. 2000a, AJ, 119, 593
Jerjen, H., Freeman, K. C., & Binggeli, B. 1998, AJ, 116, 2873
———. 2000b, AJ, 119, 166
Koekemoer, A. M., Fruchter, A. S., Hook, R. N., & Hack, W. 2002, in Proc. *HST* Calibration Workshop, Hubble after the Installation of the ACS and the NICMOS Cooling System, ed. S Arribas, A. Koekemoer, & B. Whitmore (Baltimore: STScI), 337
Kundu, A., & Whitmore, B. C. 2001, AJ, 121, 2950
Lee, J. H., Lee, M. G., & Hwang, H. S. 2006, ApJ, 650, 148
Malin, D. F., & Carter, D. 1983, ApJ, 274, 534
Maybhate, A., Goudfrooij, P., Schweizer, F., Puzia, T., & Carter, D. 2007, AJ, 134, 1729
Mei, S., Scodeggio, M., Silva, D. R., & Quinn, P. J. 2003, A&A, 399, 441
Mei, S., et al. 2005, ApJS, 156, 113
———. 2007, ApJ, 655, 144
Mieske, S., Hilker, M., & Infante, L. 2006, A&A, 458, 1013
Mould, J. R., et al. 2000, ApJ, 529, 786
Patricelli, B. 2006, *Laurea* thesis, Univ. degli studi dell'Aquila
Pence, W. D. 1986, ApJ, 310, 597
Poggianti, B. M. 1997, A&AS, 122, 399
Press, W. H., Teukolsky, S. A., Vetterling, W. T., & Flannery, B. P. 1992, Numerical Recipes in C: The Art of Scientific Computing (Cambridge: Cambridge Univ. Press)
Raimondo, G., Brocato, E., Cantiello, M., & Capaccioli, M. 2005, AJ, 130, 2625
Rekola, R., Jerjen, H., & Flynn, C. 2005, A&A, 437, 823
Riess, A. G., et al. 2005, ApJ, 627, 579
Schlegel, D. J., Finkbeiner, D. P., & Davis, M. 1998, ApJ, 500, 525
Sikkema, G., Carter, D., Peletier, R. F., Balcells, M., Del Burgo, C., & Valentijn, E. A. 2007, A&A, 467, 1011
Sirianni, M., et al. 2005, PASP, 117, 1049
Tamura, N., Kobayashi, C., Arimoto, N., Kodama, T., & Ohta, K. 2000, AJ, 119, 2134
Teodorescu, A. M., Méndez, R. H., Saglia, R. P., Riffeser, A., Kudritzki, R.-P., Gerhard, O. E., & Kleyna, J. 2005, ApJ, 635, 290
Thomsen, B., Baum, W. A., Hammergren, M., & Worthey, G. 1997, ApJ, 483, L37
Tonry, J. L., Ajhar, E. A., & Luppino, G. A. 1990, AJ, 100, 1416
Tonry, J. L., Blakeslee, J. P., Ajhar, E. A., & Dressler, A. 1997, ApJ, 475, 399
Tonry, J. L., Dressler, A., Blakeslee, J. P., Ajhar, E. A., Fletcher, A. B., Luppino, G. A., Metzger, M. R., & Moore, C. B. 2001, ApJ, 546, 681
Tonry, J., & Schneider, D. P. 1988, AJ, 96, 807
Turnbull, A. J., Bridges, T. J., & Carter, D. 1999, MNRAS, 307, 967
Udalski, A., Soszynski, I., Szymanski, M., Kubiak, M., Pietrzynski, G., Wozniak, P., & Zebrun, K. 1999, Acta Astron., 49, 223
Wang, X., Wang, L., Pain, R., Zhou, X., & Li, Z. 2006, ApJ, 645, 488
Westera, P., Lejeune, T., Buser, R., Cuisinier, F., & Bruzual, G. 2002, A&A, 381, 524
Wilkinson, A., Prieur, J.-L., Lemoine, R., Carter, D., Malin, D., & Sparks, W. B. 2000, MNRAS, 319, 977